Chinese Physics C Vol. 42, No. 11 (2018) 115001

Investigation of natural contamination layer growth on optical substrates*

Li Jiang(蒋励)[1] Qiu-Shi Huang(黄秋实)[1;1)] Igor V. Kozhevnikov[2] Yi-Yun Yao(姚逸云)[1]
Jiang-Tao Feng(冯江涛)[1] Yu-Fei Feng(冯宇飞)[1] Bin Ma(马彬)[1] Hong-Fei Jiao(焦宏飞)[1]
Hong Chen(陈鸿)[1] Zhong Zhang(张众)[1] Zhan-Shan Wang(王占山)[1;2)]

[1] Key Laboratory of Advanced Micro-Structured Materials MOE, Institute of Precision Optical Engineering,
School of Physics Science and Engineering, Tongji University, Shanghai 200092, China
[2] Shubnikov Institute of Crystallography of Federal Scientific Research Centre "Crystallography and Photonics" of
the Russian Academy of Sciences, Leninskiy pr. 59, Moscow 119333, Russia

Abstract: The surface contamination layer on mirrors can cause significant degradation of the optical performance, which is widely observed in applications, particularly in the fabrication of X-ray focusing telescopes. In this paper, we study the natural contamination layer arising from adsorption precipitation of hydrocarbons or other organic and water molecules in the absence of any external factor. Temporal evolution of the layer formed on super-smooth fused silica, borosilicate glass, and silicon substrates is studied by X-ray reflectometry, atomic force microscopy, and transmission electron microscopy for a one-year period after surface cleaning. The general characteristics of adhesion layer growth are established and discussed. The reconstructed dielectric constant profiles demonstrate that an increase in the adhesion layer thickness, deposited mass and density over time obeys power laws with extremely small exponents. Therefore, the adhesion layer growth is rapid immediately after surface cleaning, with $a \sim 1$ nm thick layer formed within the first day on all three substrates studied, while the layer density is low (~ 1 g/cm^3). The layer growth on the fused silica and silicon substrates became very slow in the succeeding days, with only a 1.4–1.5 nm thick layer and 1.2–1.3 g/cm^3 density after one year of storage in air. At the same time, the adhesion layer growth on the glass substrate showed unexpected acceleration about two months after cleaning, so that the layer thickness reached $\sim$ 2.2 nm after one year of storage. The reason for this effect, which is connected with leaching of the glass, is discussed briefly.

Keywords: X-ray telescope, surface contamination, surface dynamics, X-ray reflectometry, inverse problem

PACS: 41.50.+h, 95.55.Ka **DOI:** 10.1088/1674-1137/42/11/115001

1 Introduction

There is currently significant technical progress in X-ray astronomy, especially in the development of X-ray focusing/imaging optics. Advanced focusing telescopes with increasingly large effective area and high angular resolution are opening new possibilities in high-energy astrophysics. Several X-ray telescopes like NuSTAR [1], Astro-H [2], and Athena [3] have been launched in recent years or are in preparation now. Several X-ray missions planned in China also employ X-ray focusing optics. The enhanced X-ray Timing and Polarimetry (eXTP) project is proposed to study matter under extreme conditions by observing neutron stars and black holes in the X-ray spectral range [4]. Another approved mission, the Einstein Probe (EP), is focused on discovering new or rare types of transients, like tidal disruption events, supernova shock breakouts, high-redshift gamma-ray bursts, etc [5]. To achieve a large effective area for the telescope, the Wolter-I type structure, consisting of many axially nested mirror shells, is commonly used. In the NuSTAR telescope, the precise assembly and alignment is accomplished by graphite spacers bonded shell-by-shell with a large amount of epoxy glue. This is the method we currently adopt. For other telescopes like the ASTRO-H and the proposed X-ray Surveyor [6], epoxy is also widely used for mirror fabrication and integration [7]. The epoxy thus becomes a crucial component in the

---

Received 18 June 2018, Published online 13 October 2018

* Supported by the National Key R&D Program of China (2016YFA0401304), the National Natural Science Foundation of China (NSFC) (61621001, U1731242, U1732268) and the Ministry of Science and Higher Education of Russian Federation within the State assignment FSRC "Crystallography and Photonics" RAS

1) E-mail: huangqs@tongji.edu.cn

2) E-mail: wangzs@tongji.edu.cn

fabrication of telescope modules, because outgassing of epoxy results in the formation and growth of a contamination layer on reflective surfaces, inducing increased X-ray absorption and scattering and thus degradation of efficiency and angular resolution of the telescope [8].

To date, the study of the outgassing contamination layer was mainly focused on its influence on the optical performance of the telescope, while information about the internal structure of the layer has been unavailable [8]. The goal of our study is to analyze the temporal evolution of the internal structure of the contamination layer (its thickness, density variation with depth, chemical composition, etc.) and thus to provide the structural parameters needed for evaluation of the optical performance of telescope in any spectral range.

The study is a part of the development of an X-ray focusing telescope for future missions like eXTP. As the first step, we should develop an adequate method providing quantitative information about the evolution of the contamination layer with time. The main tool used in this study is X-ray reflectometry, which is well-suited for analysis of material structures on the nanometer scale [9]. The object chosen for the study is the natural contamination layer arising on any surface stored in air, which mainly consists of hydrocarbon and water molecules that adhere to the surface due to van der Waals forces. The importance and necessity of the first step is indicated by the following reasons.

The formation of a natural contamination layer occurs simultaneously with epoxy outgassing. It is necessary to compare and differentiate the results (e.g. the contamination layer thickness and density) of both effects, which is important for accurate evaluation of the impact of epoxy outgassing and determination of proper assembly conditions for the telescope.

The growth of a carbonaceous contamination layer is an area now under intense study as applied to the problem of degradation of optical elements placed in modern synchrotron facilities [10, 11] and free-electron laser beamlines [12], as well as in extreme ultraviolet lithography tools [13, 14]. Incoming hydrocarbon molecules, which are present even in high vacuum systems, are polymerized under the influence of highly intense radiation flux or the photoelectrons created by it, and form a stable and dense film with a thickness that increases continuously with the irradiation time and that can achieve at least tens of nanometers [10].

However, natural carbon-containing adhesion layers have been studied much less. Even the thickness of the adhesion layer as determined in different papers differs by one order of magnitude and varies from 0.6 nm [15] up to 6 nm [16], with both values being found through similar (Auger spectroscopy) techniques.

The presence of a natural adhesion layer formed on a surface in the absence of any external factor has been observed previously in a few experiments that studied the internal structure of materials by hard X-ray (HXR, photon energy E >5 keV) and soft X-ray (SXR, E <5 keV) reflectometry. In particular, the reflectivity of C-, B_4C-, and Ni-coated prototypes of X-ray free electron laser mirrors was measured in Ref. [17] versus the photon energy in a wide SXR spectral interval. A sharp decrease in the reflectivity at the absorption edge of oxygen was observed for C- and B_4C-coated mirrors and at the absorption edge of carbon for the Ni-coated one. It would appear reasonable that sharp gains in absorption are caused by the natural adhesion layer consisting of molecules of hydrocarbons or more complicated organic compounds containing carbon and oxygen, as well as molecules of water and, maybe, pure oxygen. The estimations performed in Ref. [17] give an indication of the carbon and oxygen atomic concentration ratio being approximately 3:1 inside the adhesion layer.

The authors of Ref. [18] demonstrated that it is impossible to properly describe the angular dependence of HXR reflectivity of HfO_2 films on silicon substrates without introducing the adhesion layer into the model of the reflecting media, even though a natural oxide layer on the Si substrates is taken into account. A similar conclusion was made in Ref. [19] as applied to the analysis of SXR reflectivity of TiO_2 films on Si substrates. The thickness of the adhesion layer and its maximum density, reached at the top of the sample, was demonstrated in these papers to be about 1.3 nm and 1–1.3 g/cm^3, respectively.

Nevertheless, an analysis of the natural adhesion layer growth over time was not performed in any of the above-mentioned papers, and investigation of the temporal evolution of a natural adhesion layer growing on super-smooth optical substrates is the goal of our work. It is necessary to establish its main characteristics and, in particular, to find the answers to a number of questions. How long does the natural adhesion layer growth continue? What is its maximum achievable thickness and density? How quickly does the adhesion layer appear after surface cleaning? How does the adhesion layer change the surface morphology of the substrates? Does the adhesion layer grow in the same manner on substrates of different materials? These questions will be investigated in the present paper.

Three types of super-smooth substrates are studied, namely, single crystalline silicon, boronsilicate glass, and fused silica. These materials are commonly used in X-ray mirror fabrication, the former two being the main candidates for making ultrathin mirrors with high resolution [12, 20–22]. This study is necessary not only for future analysis of epoxy outgassing contamination, but also for evaluations of substrate quality and variations in the optical parameters of mirrors and other optical elements after long-term storage.

The HXR reflectivity measurements used as the main tool for the study are described in Section 2. Reconstruction of the depth-distribution of the dielectric constant is explained in Section 3, where the problem of the uniqueness of the profiles discovered is also discussed. The basic characteristics of adhesion layer growth are presented in Section 4. The atomic force microscopy (AFM) study of the surface morphology and the subsequent transmission electron microscopy (TEM) analysis of the nanoparticles that appeared on the glass substrate are discussed in Section 5. The main results of the paper are summarized in Section 6.

2 Experiment

We analyzed the natural adhesion layer growth on three different super-smooth substrates used widely in X-ray to visible optics: fused silica (FS), silicon (100) (SI) and borosilicate glass (GL). The sample size was 20 mm ×20 mm for SI and GL and a 30 mm diameter for FS. The chemical composition of the glass was mainly SiO_2 and B_2O_3, as well as a smaller amount of oxides of alkalis and other metals including Na, K, Zn, Ti, Al, and Ca. The glass density was 2.5 g/cm^3. The root-mean-squared (RMS) roughness of all samples measured with AFM immediately after cleaning (1 ×1 μm^2 scan) was around 0.20–0.25 nm. First, the sample surfaces were cleaned by dehydrated ethanol and deionized water, and then they were kept in a clean room in the same closed plastic box in an air environment. The temperature was controlled at 20 to 23 degrees Celsius, and the air humidity was below 60%.

The reflectivity measurements were performed with a commercial laboratory diffractometer (Bruker D8) at the 0.154 nm wavelength (characteristic Cu-Kα radiation). The width of the source and detector slits was 0.2 and 1.0 mm, respectively. The measured reflectivity was normalized to the incident beam intensity. The wings of the primary beam were measured in the absence of a sample by a detector scan up to the 20° deflection angle. The measured noise level normalized to the incident intensity proved to be about 4×10^{-8} and remained unchanged during the whole one-year period of measurements. The noise was subtracted from the measured reflectivity curves, which then were averaged (at $\theta > 2.5°$) over the 0.05° angular interval to decrease statistical oscillations.

The experimental reflectivity versus the grazing angle of the incoming beam is shown in Fig. 1 (colored curves) for the three samples studied and for the different time periods during which the sample was kept in the air after surface cleaning. These periods (in days) are indicated by the numbers near the reflectivity curves. For comparison, the dotted curve represents the reflectivity calculated with the Fresnel formula, neglecting the presence of the adhesion layer and assuming a constant dielectric permittivity inside the substrate.

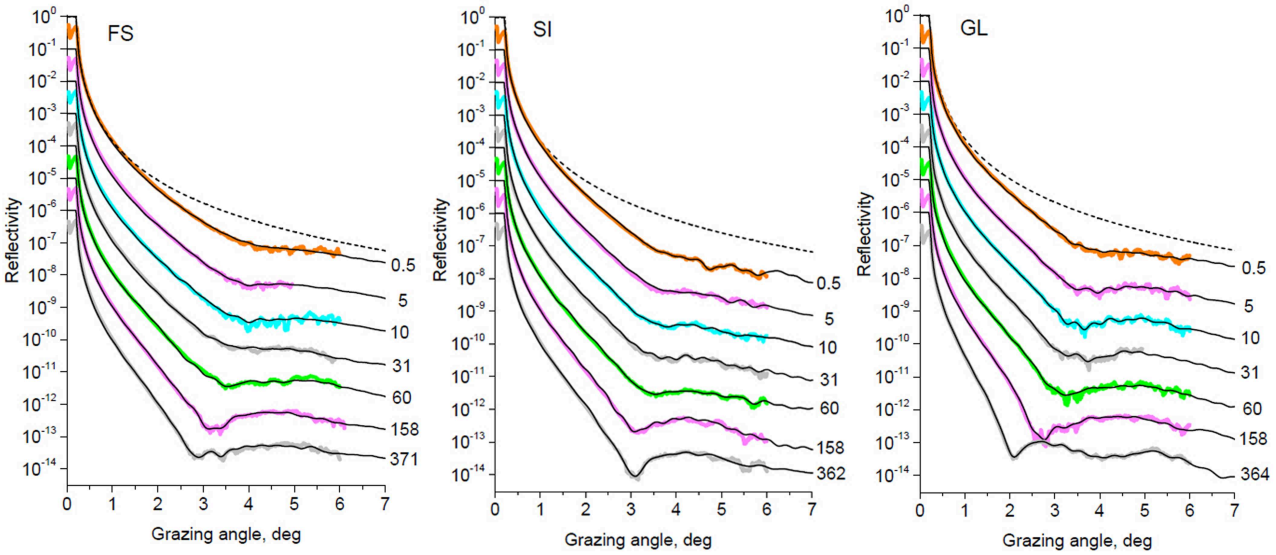

Fig. 1. (color online) The measured reflectivity (colored curves) at $\lambda = 0.154$ nm versus the grazing angle of fused silica (FS), silicon (SI) and glass (GL) samples after different time intervals exposing the sample to air. The curve number corresponds to time (in days) elapsed after the sample surface cleaning. Thin black curves demonstrate the result of calculations with the use of the dielectric constant profiles shown in Fig. 2. The curves are shifted vertically for clarity. For comparison, the Fresnel reflectivity is also presented as a dotted curve.

The figure clearly demonstrates an essential difference between the Fresnel reflectivity and the measured one, which is related to the presence of the natural adhesion layer on the substrate surface. The difference increases over time, and the well-pronounced feature (local minimum) in the reflectivity curve is shifted to a smaller grazing angle, demonstrating the growth of the adhesion layer, which still continues to grow after one year has elapsed following the surface cleaning.

3 Experimental data processing

Reconstruction of the depth distribution of the dielectric permittivity $\varepsilon(z)$ (or the electron density, which is equivalent for light materials in the hard X-ray region) was most often performed using a model of a reflecting medium with a certain number of fitting parameters. If the internal structure of the sample studied is well known a priori, the model approach allows proper reconstruction of the dielectric constant profile, although the problem of reconstruction ambiguity still persists [18]. However, if it is unknown, modeling would have a high degree of degeneracy, so the results would not be reliable as demonstrated in, e.g., Ref. [23].

In our consideration, the internal structure of fused silica and silicon substrates is well-known, and the model approach could most likely be applied for analysis of the adhesion layer growth. However, the glass substrate is characterized by surface leaching [24, 25], i.e., chemical reactions between the oxides composing the glass (Na_2O, K_2O, etc.,) and the water molecules contained in the polishing suspension and/or in the atmospheric air, which results in the appearance of combined alkalis (NaOH, KOH, etc.,) which exist in the subsurface layer. Thus, the shape of the dielectric constant profile inside the leached layer and even its thickness is unknown, as it depends on the chemical composition of the glass and the fabrication technology of the substrates [24, 26]. Therefore, in our analysis we used the model-independent approach developed earlier in Ref. [27, 28].

The approach is based on very general assumptions about a layered medium reflecting X-rays. As applied to our problem and according to the general considerations described in Ref. [27], we can indicate the following important features for the measured reflectivity. First, the reflectivity curves of all samples are congruent with the Fresnel reflectivity at large grazing angles θ, i.e., they decrease as $1/\sin^4\theta$. This means that there are particular points where the dielectric constant changes abruptly. Second, we do not observe periodic oscillations of the reflectivity with the grazing angle, i.e., we suggest that there is only one particular point in the dielectric constant profile. We assume that this point corresponds to a substrate surface placed at $z=0$, where the Z-axis is directed into the substrate depth, the dielectric permittivity $\varepsilon(z)$ varying smoothly and tending to the constant value ε_{sub} in the substrate depth. As the chemical composition and density of the substrates are known, the value of ε_{sub} can be calculated [29]. Third, we assume that there is an adhesion layer on the substrate surface, its density decreasing smoothly in a vacuum and tending to a zero value with increasing distance from the substrate surface. These statements determine the general model used in our calculations. Then, the main term of the asymptotic expansion of the reflectivity at large grazing angles θ has the following form [27]:

$$R(\theta\gg\theta_c)\cong\frac{|\Delta|^2}{16\sin^4\theta},$$

where

$$\Delta\equiv\varepsilon(+0)-\epsilon(-0)\neq0 \tag{1}$$

Notice that the value $1-\varepsilon_{\text{sub}}$ determines the critical angle θ_c of the total external reflection (TER), while the variation in the dielectric constant Δ at the peculiar point $z=0$ determines the asymptotic behavior of the reflectivity (1). In general, the value of Δ can be found directly from the experimental reflectivity curve, if the measurements are performed at a wide-enough interval of the grazing angle.

Therefore, among an infinite number of possible solutions of the inverse problem of X-ray reflectometry, i.e., different dielectric constant profiles describing the reflectivity curve in the measurable interval of the grazing angles within the prescribed accuracy, we should choose those of them that provide the asymptotic dependence of the reflectivity $R(\theta)\sim1/\sin^4\theta$ outside the measurable angular range, the value of Δ being unnecessary for algorithm operation and being found from the fitting procedure. In other words, even though the reflectivity is being measured within a limited interval of the grazing angle, we extend it in a physically reasonable manner to the whole range of θ. This is the key feature of our approach, allowing a considerable decrease in the number of possible solutions of the inverse problem and the acquisition of a unique solution on frequent occasions [27, 28].

In addition, we neglect the absorption of X-rays in the matter. Otherwise, it is necessary to determine two a priori unknown functions $\mathrm{Re}[\varepsilon(z)]$ and $\mathrm{Im}[\varepsilon(z)]$, which, in general, are independent of each other, so that the problem of ambiguity of the inverse problem solution becomes much more difficult.

In fact, the influence of hard X-ray absorption on the reflectivity of a thin layer on a substrate, as in our case, is negligible except for extremely small grazing angles lying inside or near the TER region. Therefore, when processing, we took into consideration only a part of the reflectivity curve, where the reflectivity value is less than

10^{-3}, i.e. we did not take into account the interval of small grazing angles less than 0.60-0.63 degrees. This was done to guarantee a negligible absorption effect on the reflectivity and to provide a beam footprint smaller than the sample size. As one can see in Fig. 1, all the reflectivity curves are very close to the Fresnel reflectivity in this angular interval, which thus does not contain essential information about depth-distribution of the dielectric constant, except for the value of the critical angle of TER, the latter being determined by the value of the dielectric constant in the substrate depth. However, the density and chemical composition of all substrates are known, and hence the dielectric constant in the substrate depth is also known a priori.

Finally, the representation (1) of the reflectivity at large grazing angles means that the effect of the roughness on the reflectivity is negligibly small in the measurable angular interval, at least. The fact is that we measured the sum R_Σ of the specular reflectivity and the total integrated scattering (TIS) in a vacuum, rather than the specular reflectance, as the detector slit was wide enough (1 mm) to collect most of the radiation scattered by long-scale roughness, which is characterized by the greatest height. As discussed in Refs. [30, 31], the long-scale roughness does not increase the radiation flux into the matter, and thus the R_Σ value is very close to the reflectivity of a perfectly smooth surface. This diffraction regime occurs if the angular width of the scattering dia-

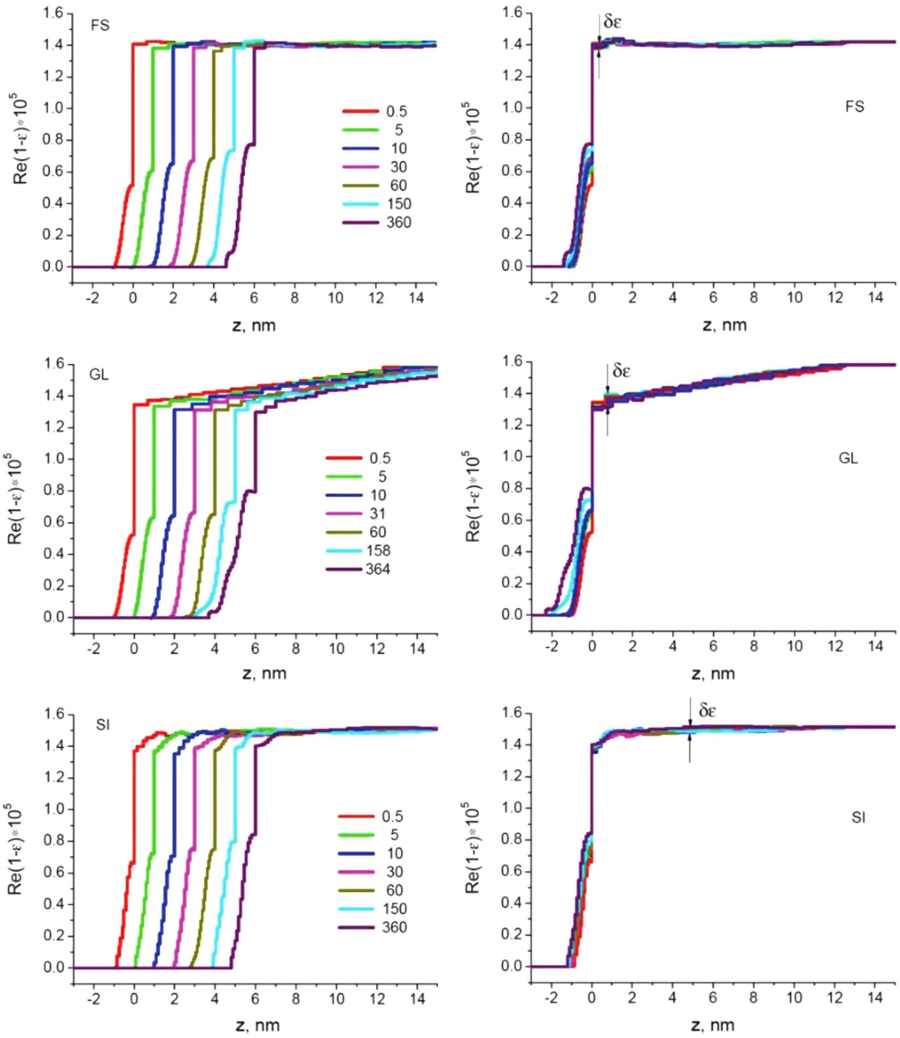

Fig. 2. (color online) The reconstructed dielectric constant profiles of fused silica (FS), silicon (SI) and glass (GL) samples after different time intervals exposing the sample to air. The curve number corresponds to time (in days) elapsed after the sample surface cleaning. The profiles are shifted horizontally in the left-hand column, while the substrate surface position is placed at the same point $z=0$ in the right-hand column. The arrows in the right-hand column indicate the maximum difference in the profiles inside the substrates.

gram in the incidence plane $\lambda/(\pi\xi\theta_0)$ essentially exceeds (by a factor of 3, at least) the grazing incidence angle θ_0. Here, ξ is the roughness correlation length, which as a rough approximation can be identified as the typical longitudinal size of the roughness. Setting the grazing incidence angle to its maximal value $\theta_0=6°$, when the roughness effect on the specular reflectance is greatest, we conclude that the roughness can be considered to be long-scale and its effect on the R_Σ value is weak, if its longitudinal size ξ >45 nm. Only high-frequency roughness (ξ <45 nm), whose height is typically very small, affects the R_Σ value as the TIS tends to zero at $\xi\to 0$, while the specular reflectance decreases due to the increasingly coherent transmittance of X-rays deep into the matter.

A detailed description of our model-free approach, the fitting procedure and the choice of the merit function providing the necessary asymptotic behavior of the reflectivity, the discussion of the calculation algorithm, analysis of the roughness effect on the dielectric constant reconstruction as well as examples of the model and experimental reconstruction of the dielectric constant profiles, are given elsewhere [23, 27, 28, 30].

The reconstructed dielectric constant profiles of all the samples studied (FS, GL, SI) are shown in Fig. 2, where the curve number indicates the time (in days) that a sample was exposed to air after cleaning. The profiles are shifted horizontally in the left-hand column to clearly observe the temporal variation in the dielectric constant inside the adhesion layer, while the substrate surface position is placed at the same point $z=0$ in the right-hand column to demonstrate the difference between the reconstructed profiles inside the substrates. The position of the maximal difference $\delta\varepsilon$ is indicated by arrows. We believe that the substrate interior is unchanged with a growth in the adhesion layer and thus the value $\pm\delta\varepsilon/2$ characterizes an error in determination of the dielectric constant profile.

The reconstructed profiles look quite reasonable from a physical point of view. An adhesion layer is thin (1–2 nm) and its thickness increases monotonically over time as expected. The layers are loose with a low maximum density of about 1.3 g/cm^3 observed for all three substrates after one year of storage in air (see the next section for more details), and the value corresponds to the data obtained in Ref. [17]. The dielectric permittivity is constant inside the fused silica substrate, while a thin oxide layer of about 1.5–2 nm thickness is observed on the surface of the Si substrate. The glass substrate is characterized by the presence of a rather thick (~11–12 nm) subsurface layer caused by surface leaching. Notice that the thickness of a leached subsurface layer depends strongly on the chemical composition of the glass and according to Ref. [26] can vary in the 3–15 nm interval, at least.

The accuracy of the reflectivity fitting is demonstrated by the black curves in Fig. 1. The calculated curves describe the experimental reflectivity well in the measurable range of the grazing angle and they are congruent with the Fresnel reflectivity outside it. The calculated GL curve, exposed for 360 days to air, is also parallel to the Fresnel one at θ >7.3°.

Next, we analyze the problem in more detail, which was not discussed before, but which can essentially influence the dielectric constant profile reconstruction. We can only find the dielectric constant in the limited interval of $z\in[z_{\min}z_{\max}]$, putting $\varepsilon(z>z_{\max})=\epsilon_{\text{sub}}=\text{const}$ and $\varepsilon(z<z_{\min})=1$, so that the values of $z_{\min}$ and $z_{\max}$ should be properly chosen to correctly reconstruct the depth distribution of the dielectric permittivity.

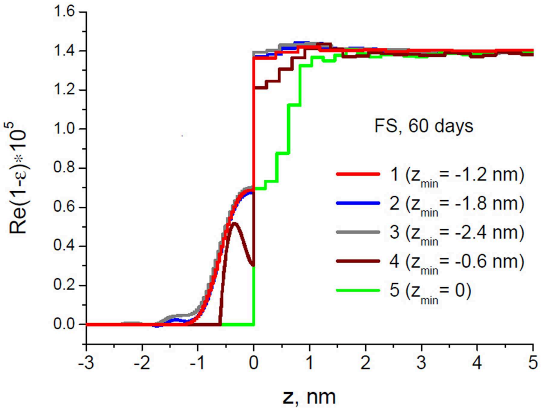

Fig. 3. (color online) Illustration of the $z_{\min}$ value effect on the shape of the reconstructed dielectric constant profile of the fused silica sample after 60 days' exposure to air.

The reconstructed dielectric constant profile (FS sample after 60 days exposure to air) is shown in Fig. 3 for different values of $z_{\min}$. If $z_{\min}=-1.2$ nm (curve 1), the adhesion layer density decreases into a vacuum in a monotonic manner and the dielectric constant of the substrate is practically constant. If $z_{\min}$ is decreased (curves 2 and 3), the shape of the adhesion layer as a whole remains the same, while the weakly pronounced oscillations around the zero value of the polarizability Re$(1-\varepsilon)$ appear at $z<-1$ nm, with the oscillation amplitudes increasing with decreasing $z_{\min}$. On the other hand, if $z_{\min}$ is increased up to -0.6 nm (curve 4), the shape of the dielectric constant profile is strongly deformed inside both the adhesion layer and the near surface layer of the substrate. Finally, if we neglect the presence of the adhesion layer on the substrate top, i.e., put $z_{\min}= 0$, we obtain curve 5 in Fig. 3, demonstrating the unphysical value of the polarizability near the sample surface, which represents only half of that in the sample depth.

Therefore, we choose the optimal $z_{\min}$ value as that with the lowest possible magnitude, which still (a) keeps the shape of the adhesion layer profile, (b) excludes the unphysical oscillations resulting in negative polarizability of the substrate, and (c) provides physically reasonable behavior of the dielectric constant profile inside the substrate. As applied to the case considered in Fig. 3, the value of $z_{\min}= -1.2$ nm is considered to be the most plausible.

Notice that profiles 1, 4 and 5 in Fig. 3 provide the same accuracy for the reflectivity fitting in the measurable interval of the grazing angle and the same asymptotic behavior of the reflectivity at larger θ, demonstrating once again an ambiguity of the dielectric constant profile reconstruction.

A similar consideration is used to choose the optimal value of $z_{\max}$ as the minimum possible one, which keeps the shape of the dielectric constant profile both in the adhesion layer and in the near surface layer of the substrate. As applied to the glass sample, the value of $z_{\max}=$ 13 nm is considered to be optimal, allowing adequate reconstruction of the leached subsurface layer, which is 11–12 nm thick. The same value for $z_{\max}$ was used in the analysis of the fused silica and glass samples in order to provide similar conditions for the dielectric constant reconstruction, while the subsurface layer is much thinner, if it ever exists in these samples.

The crucial problem in X-ray reflectometry is a justification of the correctness of the reconstructed dielectric constant profile. The problem is that the mathematical theorems guaranteeing the uniqueness of the solution imply that the phase of the amplitude reflectivity is measured in parallel to its absolute value. However, information about the reflectivity phase is lost in conventional X-ray experiments. In this respect, we would indicate Refs. [32, 33], where the method for the phase determination from conventional reflectivity measurements is described, though it requires the calculation of the temporal derivative $\mathrm{d}R/\mathrm{d}t$. However, the noise in our reflectivity curves, measured with a laboratory diffractometer, is too high to apply this approach.

As discussed in Refs. [20, 27], the most realistic solution to the inverse problem can be found on the basis of a simultaneous analysis of several similar samples, which differ only slightly from each other. In particular, in the case of film coatings having different thicknesses deposited onto identical substrates, the reconstructed dielectric constant profiles should be the same in the substrate interior. Actually, Fig. 2, in the right-hand column, demonstrates the identity of the reconstructed internal substrate structure even though the reflectivity curves (Fig. 1) are essentially changed over time, because of the adhesion layer growth. The differences between the profiles in the substrate's interior is only of the order of 2%–4% of the value of the dielectric constant in the substrate depth, i.e., essentially less than the stochastic variations in the reflectivity at large grazing angles. This is reasonable since the algorithm we used is very stable with respect to random reflectivity fluctuations [27]. Because the substrate's interior is reconstructed properly, we can conclude that the adhesion layer's profile was also identified correctly.

One more argument in support of the accuracy of the profiles that were found is the physically reasonable behavior of the reflectivity outside the measured interval of the grazing angle. The importance of this statement is illustrated by Fig. 4. Curve 2 in Fig. 4(a) demonstrates the accuracy of the fitting of the whole experi-

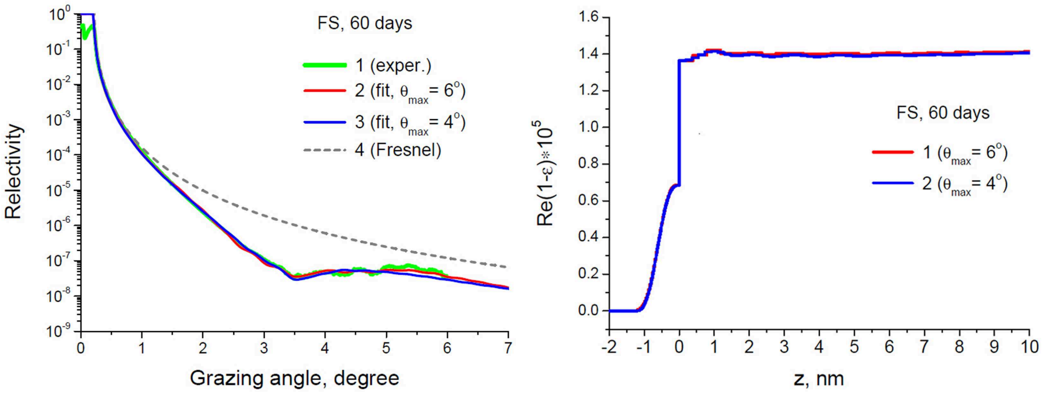

Fig. 4. (color online) (a) The measured reflectivity (curve 1) of the fused silica sample after 60 days' exposure to air. The fitting results are shown by curves 2 and 3, with the reflectivity measured up to 6° or 4° taken into account, respectively. The Fresnel reflectivity (curve 4) is also shown for comparison. (b) The reconstructed dielectric constant profiles, when the reflectivity measured up to 6° (curve 1) or 4° (curve 2) is taken into account.

mental reflectivity (curve 1) measured up to the grazing angle $\theta_{\max}= 6°$, the reconstructed dielectric constant profile being shown by curve 1 in Fig. 4(b). Then we take into account only part of the experimental reflectivity curve up to $\theta_{\max}= 4°$ and reconstruct the dielectric constant profile again. The calculated reflectivity is shown in Fig. 4(a), curve 2. As seen, curve 2 practically coincides with curve 1 at all grazing angles including the large angle $\theta > 4°$, i.e. the approach allows us to correctly predict the reflectivity outside the measurable interval of the grazing angles. Moreover, the reconstructed profile (curve 2 in Fig. 4(b)) is not changed at all as compared with the previous case (curve 1), when the measured reflectivity up to the 6° grazing angle is taken into account. These facts justify the validity of our approach and the accuracy of the reconstructed profiles.

4 Discussion

The real part of the dielectric permittivity of a material consisting of several chemical elements is expressed in the X-ray region as [34]

$$\mathrm{Re}(1-\varepsilon)=\frac{r_0\lambda^2}{\pi}\sum N_j f_j(\lambda),$$

where N_j and f_j are the specific concentration and the real part of the atomic scattering factor of the jth element comprising the material, respectively, and r_0 is the classical electron radius. For practical calculations the last expression is conveniently rewritten as

$$\mathrm{Re}(1-\varepsilon)=0.54\cdot10^{-3}\lambda^2\rho\frac{\sum\alpha_j f_j(\lambda)}{\sum\alpha_j\mu_j}, \tag{2}$$

where the wavelength λ is in nm, the material density ρ is in g/cm3, the atomic weight μ_j is in atomic mass units, and α_j is the relative atomic concentration of the jth element ($\sum\alpha_j=1$).

For light chemical elements in the hard X-ray region, $\mu\approx 2Z$ and $f\approx Z$, where Z is the atomic number of a chemical element. In particular, $\mu= 12.011$ and $f=6.02$ for carbon ($Z=6$), and $\mu= 15.9994$ and $f= 8.05$ for oxygen ($Z= 8$) at the working wavelength $\lambda= 0.154$ nm [29]. Then, we immediately find from Eq. (2) that the depth distribution of the adhesion layer density (in g/cm^3) can be deduced from the experimental dielectric constant profile as

$$\rho(z)\approx1.56\cdot10^{-3}\mathrm{Re}[1-\varepsilon(z)] \tag{3}$$

with an accuracy better than 0.6 %.

Then we can find the mass of the adhesion layer de-

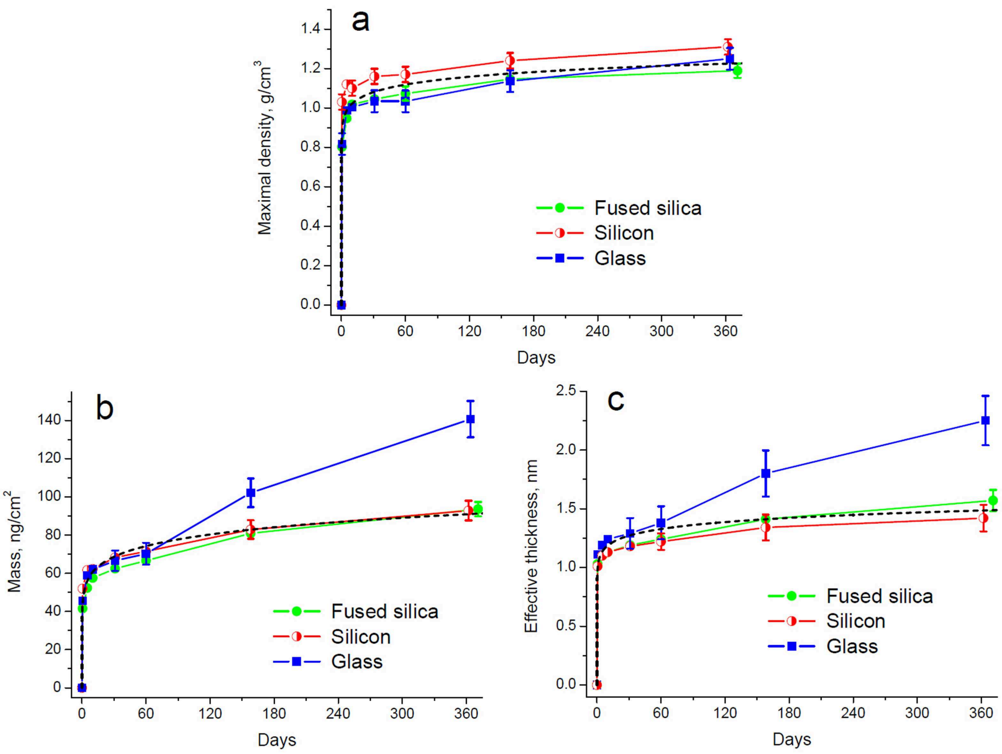

Fig. 5. (color online) Increase in (a) the maximum density, (b) mass deposited onto the unit surface area, and (c) effective thickness of the adhesion layer over the time elapsed after surface cleaning. The dashed curves demonstrate the result of fitting with the use of the model (6).

posited on a unit surface area

$$m=\int_{z_{\min}}^{0}\rho(z)\mathrm{d}z \tag{4}$$

and the effective layer thickness d_{eff} determined via the relation

$$m=d_{\mathrm{eff}}\cdot\rho_{\max}/2, \tag{5}$$

where $\rho_{\max}$ is the maximum density of the adhesion layer achieved at the substrate surface. Relation (5) corresponds to an approximation of the adhesion layer profile by a triangle with height $\rho_{\max}$ and base d_{eff}.

An increase in the maximum density, the deposited mass and the effective thickness of the adhesion layer with time elapsed after substrate cleaning is shown in Fig. 5. The error indicated in the figure relates to the inaccuracy $\pm\delta\varepsilon/2$ in the dielectric constant profile reconstruction (see Fig. 2). The figure demonstrates that the adhesion layer grows identically (within the experimental error) on fused silica and silicon substrates. The adhesion layer growth on the glass substrate also occurs in the same manner within 60 days after the substrate cleaning, but the growth rate is essentially enhanced later. The reason is explained below.

Assuming that the original adhesion layers were completely removed by the cleaning procedure, the experimental curves $m(t)$, $\rho_{\max}(t)$, and $d_{\mathrm{eff}}(\mathrm{t})$ can be described adequately by the following power law dependences:

$$d_{\mathrm{eff}}(t)=\left(\frac{t}{t_0}\right)^{\eta_d}, \qquad m(t)=\left(\frac{t}{t_0}\right)^{\eta_m},$$
$$\rho_{\max}(t)=0.02m_0\left(\frac{t}{t_0}\right)^{\eta_m-\eta_d}, \tag{6}$$

where d_{eff} is in nm, m is in ng/cm^2, and $\rho_{\max}$ is in g/cm^3. The fitting was performed for all three samples at once, excluding the two last experimental points (at $t>60$ days) for the glass sample. The results of the fitting are shown in Fig. 5 (dashed curves).

The fitting parameter $t_0\approx0.6491$ days characterizes the time necessary for the effective thickness of the adhesion layer to achieve 1 nm. The parameter $m_0\approx44.51$ ng/cm^2 determines the mass deposited onto the surface during this period. The next two dimensionless parameters $n_d\approx0.06259$ and $\eta_m\approx0.1131$ are very small as compared with unity, and thus demonstrate very quick growth of the adhesion layer immediately after surface cleaning, while the growth is very slow at $t>t_0$ due to a concurrence between two opposite processes – adsorption and desorption of hydrocarbon molecules. In particular, if we extrapolate Eqs. (6) to a 10-year period for a sample kept in air, we find that the effective thickness of the adhesion layer on silicon and fused silica substrates would increase up to only 1.72 nm, the deposited mass up to 118 ng/cm^3, and the maximum density up to 1.38 g/cm^3. Notice that the deposited mass increases quicker than the effective thickness because of the increasing density of the adhesion layer over time.

If the original adhesion layer is completely removed by the cleaning procedure and Eq. (6) is valid at the initial stage of adhesion layer growth, we estimate that the layer reaches 0.4 nm thickness (one to two monolayers of organic molecules) after only $t=24.6$ ms, while the layer density $\rho_{\max}=0.425$ g/cm^3 is very low. In other words, the adhesion layer at the initial stage of its growth can represent an ephemeral construction of weakly bonded hydrocarbon and other organic molecules with large voids between them, rather than a conventional uniform bulk film. The molecules are more closely packed with the growth of the adhesion layer, whose density is thus increased.

Notice that experimental study of the earliest stage of adhesion layer growth runs into two problems of a fundamental nature. First, it is necessary to measure the reflectivity curve immediately within a small fraction of a second after surface cleaning. Second, the minimum thickness of a feature placed on a substrate surface, which can still be reconstructed correctly, is of the order of $\lambda/(2\sin\theta_{\max})$ according to the analysis performed in Ref. [27] and thus it is equal to about 0.75 nm in the conditions of our experiment. Hence, the reflectivity should be measured up to essentially larger grazing angle $\theta_{\max}$, and the experimental noise level should be much lower. The only method that we can imagine would be in situ reflectivity measurements with a synchrotron source, performed in an ultrahigh vacuum to decrease the rate of the adhesion layer growth by several orders of magnitude. However, it is not evident that the growth of the adhesion layer in a vacuum obeys the same principles as growth in air.

5 AFM and TEM study of the sample surface structure

To observe the variation in the surface morphology over the time elapsed after cleaning, the samples were studied with AFM. The measurements were performed on three different surface areas of $1\times1\,\mu\mathrm{m}^2$ size (256×256 measurement points). The results are shown in Fig. 6. The surfaces of all the samples measured immediately after cleaning (~ 0.5 day after cleaning) were very smooth, with an RMS roughness of about 0.25 (SI and GL samples), and 0.20 nm (FS sample). The peak-to-valley (PV) variation in the surface profile is 1.9 to 2.3 nm for the different samples

After 9.5 months of storage, the RMS roughness of the SI and FS surfaces remained unchanged and equal to about 0.25 nm and 0.19 nm, respectively. A few tiny particles were observed on the surface, which can be explained as dust contamination from the exposure to air occurring during the X-ray reflectivity and AFM

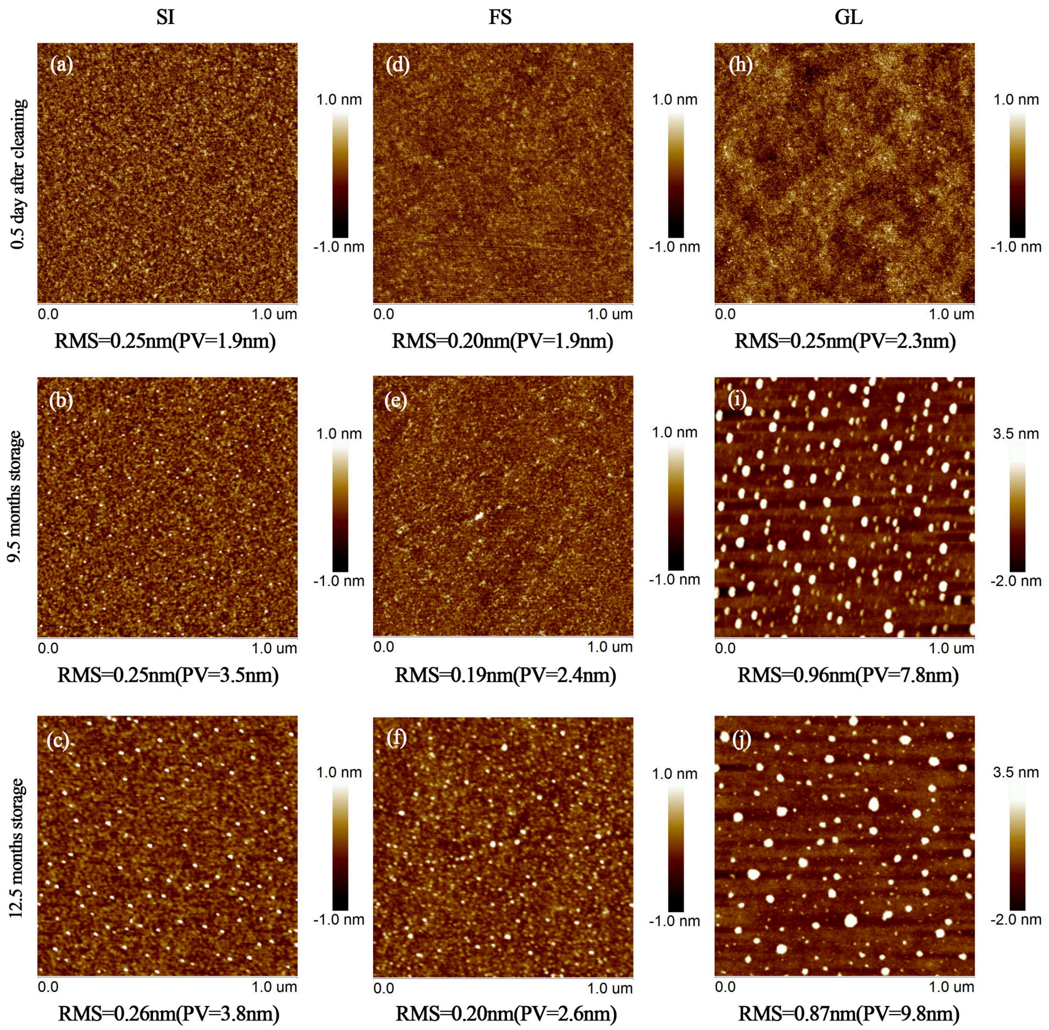

Fig. 6. (color online) AFM images of the surface of the silicon (column SI, (a), (b), (c)), fused silica (column FS, (d), (e), (f)), and glass (column GL, (h), (i), (j)) samples after different storage times in air (0.5 days, 9.5 and 12.5 months). The images of the Si and fused silica samples share the same color scale.

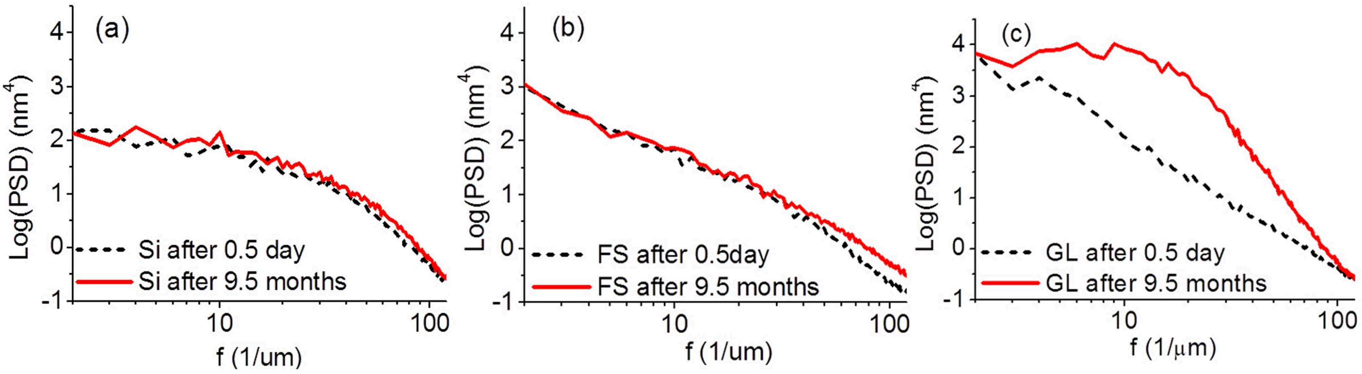

Fig. 7. (color online) 2D PSD-functions of (a) Si, (b) fused silica, and (c) glass surfaces after 0.5-day (dashed line) and 9.5-month (solid line) storage in air.

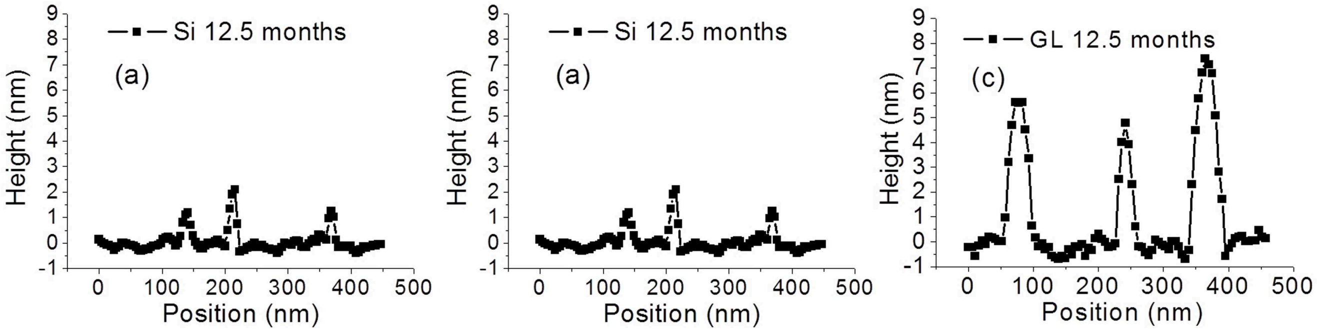

Fig. 8. (color online) Typical AFM line profiles across the surface particles on the (a) Si, (b) fused silica, and (c) glass samples after one year of storage.

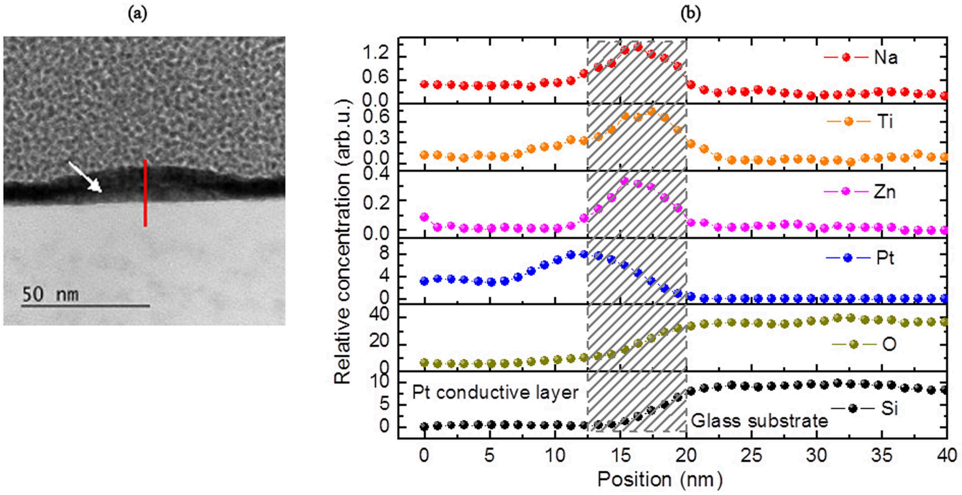

Fig. 9. (color online) (a) TEM image of a single particle on the glass surface. The red line indicates the EDX line scan. (b) Relative concentration of the chemical elements along the EDX scan. The shaded region corresponds to the interior of the particle. The abscissa axis is directed into the glass substrate depth.

measurements performed outside the clean room. The PV value increased slightly to 3.5 and 2.4 nm for the SI and FS samples, respectively. The two-dimensional power spectral density (PSD) functions measured with AFM at 0.5 day and 9.5 months after cleaning are shown in Fig. 7. The PSD-functions of the SI (Fig. 7(a)) and FS (Fig. 7(b)) samples remained practically unchanged during the 9.5 months of storage.

However, the surface structure of the GL sample was drastically changed: a large number of particles appeared on the surface of the GL sample with a height of around 2–6 nm and a lateral size of 20–40 nm after 9.5 months' storage (Fig. 6). The PV value was significantly increased, to 7.8 nm. Similarly, the PSD-function of the GL sample shown in Fig. 7(c) increased dramatically in the spatial frequency range of f ∼ 5–50 μm^{-1}. Notice that three GL samples were studied with AFM and a similar phenomenon was observed on the surfaces of all of them.

After one year of storage, the dust contamination was slightly increased on the SI and FS surfaces, while the RMS roughness and the PV value remained almost the same as before. The particles on the GL surface demonstrated further development up to a height of 3–8 nm and a lateral size of 20–55 nm, with a PV value of 9.8 nm. Typical line profiles across the surface of all three samples studied are shown in Fig. 8, demonstrating once again a similar surface morphology for the FS and SI samples after 1 year of storage and the quite different surface structure of the GL sample, related to the appearance of relatively large particles on the surface. These particles represent a high-frequency surface roughness affecting the X-ray reflectivity in the same manner as a smooth variation in the dielectric constant at the substrate–vacuum interface. As a result, an essential increase in the contamination layer thickness is observed in the reconstructed dielectric constant profiles starting from about two months elapsed after cleaning (Figs. 2, 5).

For a better understanding of particle growth on a glass surface, we used transmission electron microscopy (TEM) and energy dispersive X-ray spectroscopy (EDX). The TEM sample was prepared by a focused ion beam (FIB). Because glass is a nonconductive material, a thin Pt layer was first deposited on the top of the sample. After the FIB preparation, a sample cross section was analyzed with TEM, and a few particles were clearly seen on the substrate surface. A bright field image of one of the surface particles (lateral size $\sim$ 60 nm, height $\sim$ 7 nm) is shown in Fig. 9(a). An EDX line scan was performed across the particle area (red line in Fig. 9(a)) to analyze the chemical composition near the surface. The concentration profiles of several typical elements are shown in Fig. 9(b). In the absence of a standard calibrated sample, only the relative concentration of elements can be measured. The abscissa axis in Fig. 9(b) is directed into the substrate depth. The shaded transition area between two asymptotic values of Pt and Si concentrations corresponds to the interior of the particle. The width of the transition area is about 7.5 nm and is consistent with the height of the particle. As can be seen, the concentration of Na, Ti, and Zn inside the particle exceeds that in the glass substrate.

According to current understanding [24, 25], atmospheric water penetrates into the glass substrate as H_2O molecules or OH$-$ groups and interacts with metal oxides, transforming them to hydroxides. The hydroxide molecules diffuse to the outside of the glass, resulting in the emergence of a so-called fused silica-like subsurface layer 3 to 15 nm thick [24, 26]. Therefore, it is not accidental that the dielectric constant value on a glass surface agrees well with that of the fused silica sample (Fig. 2). Figures 6 and 9 demonstrate that the hydroxide molecules escaping from the glass substrate form agglomerates on its surface. As the leaching process continues over time, the size of the surface particles gradually increases with the time elapsed after glass substrate cleaning. Therefore, we would expect that the shape of the dielectric constant profile inside the leached layer to vary slightly as well during the progression of the experiment. Maybe this is a reason why the different $\delta\varepsilon$ in the reconstructed dielectric constant profiles near the glass substrate surface (Fig. 2) is doubled compared with that near the fused silica and silicon surfaces.

6 Conclusions

The temporal evolution of the natural adhesion layer formed on super-smooth fused silica, borosilicate glass, and silicon substrates was studied over a one-year period after chemical cleaning. X-ray (HXR) reflectometry (λ= 0.154 nm) was the main tool for the study, in which the reconstruction of the depth distribution of the dielectric permittivity near the surface was performed with the use of a model-free approach. The reconstructed dielectric constant profiles demonstrated increases in the thickness, density, and mass of the adhesion layers over the time elapsed after surface cleaning, and these increases continued after one year of storage of the samples in air. Assuming that the original adhesion layer was completely removed by the cleaning procedure, its growth was estimated to be very fast immediately after surface cleaning, with $a\sim$1 nm thick layer formed within the first day on all three substrates, while the layer density was low ($\sim$ 1 g/cm^3). The layer growth on the FS and SI substrates became very slow in the succeeding days with only a 1.4–1.5 nm thick layer and 1.2–1.3 g/cm^3 density appearing after one year of air storage. The surface morphology (the PSD-function and the RMS roughness) of the FS and SI samples was shown to be almost unchanged after one year of storage in air, in spite of the presence of an adhesion layer on the top.

However, the adhesion layer growth on the GL substrate demonstrated unexpected acceleration after about 2$\sim$ 5 months elapsed after cleaning, so that the adhesion layer thickness reached 2.2 nm after one year of storage. This phenomenon was explained by the appearance of relatively large nano-particles on the surface, resulting in an essential enhancement of the roughness and the PSD-function in the high-frequency region as compared with the FS and SI samples. The TEM and EDX analysis demonstrated that the particles contained the same metals as the glass, which can be explained by the interaction between the atmospheric water molecules (penetrating into the glass substrate) and the metal oxides in the glass, transforming them into hydroxides (glass leaching) with subsequent outward diffusion and agglomeration of the hydroxide molecules on the glass surface.

The results obtained in the present paper will be useful for the analysis of future experiments on contamination layer growth caused by epoxy outgassing during the assembly of X-ray telescopes, since the effect of natural contamination can be evaluated separately. Moreover, the HXR reflectometry tool can be used to characterize the structure of other surface contamination layers on different mirrors e.g. those used for synchrotron radiation facilities. It can provide important guidance for quality evaluation of optical substrates and elements after long-term storage.

References

1 C. J. Hailey, H. J. An, K. L. Blaedel et al, Proc. SPIE, 7732-28 (2010)

2 Y. Soong, T. Okajima, P. J. Serlemitsos et al, Proc. SPIE, **9144**: 914428 (2014)

3 M. Bavdaz, E. Wille, M. Ayre et al, Proc. SPIE, **10399**: 103990B (2017)

4 S.N. Zhang, M. Feroci, A. Santangelo et al, Proc. SPIE, **9905**: 99051Q-1 (2016)

5 W.M. Yuan, C. Zhang, Y. Chen et al, Sci Sin-Phys Mech Astron, **48**: 039502 (2018)

6 S. L. O'Dell, R. Allured, A. O. Ames et al., Proc. SPIE, **9965**: 996507 (2016)

7 K.W. Chan, W. W. Zhang, M. J. Schofield et al, Proc. SPIE, **9905**: 99056X (2016)

8 H. J. An, F. E. Christensen, M. Doll et al, Proc. SPIE, **7437**: 74371J-1 (2009)

9 M.Tolan, In Springer Tracts in Modern Physics, Vol. 148, (Berlin: Springer, 1999)

10 K. Boller, R.-P. Haelbich, H. Hogrefe et al, Nucl. Instrum. Methods A, **208**: 273-279 (1983)

11 Q. S. Huang, H. C. Li, Z. Q. Song et al, Chin. Phys. C, **37**(2): 028002 (2013)

12 I. V. Kozhevnikov, A. V. Buzmakov, F. Siewert et al, J. Synchr. Rad., **23**: 78-90 (2009)

13 J. Chen, E. Louis, C. J. Lee et al, Opt. Express, **17**: 16969-16979 (2009)

14 Q. S. Huang, V. Medvedev, R. van de Kruijs et al, Appl. Phys. Rev., **4**: 011104 (2017)

15 R. Bouwman, J. B. van Mechelen, A. A. Holscher, In Surface Contamination. Genesis, Detection, and Control, Vol. 1, (Plenum Press, NY), 87-296 (1978)

16 H. B. Bonham, P. V. Plunkett, In Surface Contamination. Genesis, Detection, and Control, Vol. 1, (Plenum Press, NY), 271-285(1978)

17 I. V. Kozhevnikov, E. O. Filatova, A. A. Sokolov et al, J. Synchrotron Rad., **22**: 348-353 (2015)

18 Y. O. Volkov, I. V. Kozhevnikov, B. S. Roshchin et al, Crystallogr. Rep., **58**: 160–167 (2013)

19 E. O. Filatova, I. V. Kozhevnikov, A. A. Sokolov et al, Sci. Technol. Adv. Mater., **13**: 015001-12 (2012)

20 K. L. Mittal, ed, In Surface Contamination. Genesis, Detection, and Control, Vol. 1., (Plenum Press, NY, 1978)

21 S. Ma, M. W. Wen, Z. S. Wang, Chin. Phys. C, **40**(7): 079001 (2016)

22 F. F. Wang, J. T. Zhu, Q. Zhong et al, Chin. Phys. C, **36**(9): 909-914 (2012)

23 E. O. Filatova, A. A. Sokolov, I. V. Kozhevnikov, Chapter 7 in the book "High-k Gate Dielectrics for SMOS Technology". Gang He, Ed. Wiley-VCH Verlag, (Weinhem, Germany), 225-271 (2012)

24 P. B. Adams, In Surface Contamination. Genesis, Detection, and Control, Vol. 1., (Plenum Press, NY), 327-338(1978)

25 R. Conradt, J. Am. Ceram. Soc., **91**: 728–735 (2008)

26 L. L. Hench, E. C. Ethridge, In Surface Contamination. Genesis, Detection, and Control, Vol. 1, (Plenum Press, NY), 313-326 (1978)

27 I.V. Kozhevnikov, Nucl. Instrum. Methods A, **508**: 519-541 (2003)

28 I.V. Kozhevnikov, L. Peverini, and E. Ziegler, Phys. Rev. B, **85**: 125439 (2012)

29 Index of refraction in the X-ray region, http://henke.lbl.gov/optical_constants/getdb2.html.

30 I. V. Kozhevnikov, Crystallogr. Rep., **57**: 490-498 (2012)

31 M. W. Wen, I.V. Kozhevnikov, Z. S. Wang, Opt. Express, **23**: 24220-24235 (2015)

32 I. V. Kozhevnikov, L. Peverini, E. Ziegler, Opt. Express, **14**: 144-149 (2008)

33 I. V. Kozhevnikov, L. Peverini, E. Ziegler, J. Appl. Phys., **104**: 054914 (2008)

34 D. Attwood, In Soft X-Rays and Extreme Ultraviolet Radiation: Principles and Applications, Cambridge University Press, Cambridge, UK, 1999